AJNR

Head and Neck Paragangliomas: Improved Tumor Detection Using Contrast-Enhanced 3D Time-of-Flight MR Angiography As Compared with Fat-Suppressed MR Imaging Techniques

René van den Berg, Berit M. Verbist, Bart J. A. Mertens, Andel G. L. van der Mey and Mark A. van Buchem

AJNR Am J Neuroradiol 2004, 25 (5) 863-870
http://www.ajnr.org/content/25/5/863

Head and Neck Paragangliomas: Improved Tumor Detection Using Contrast-Enhanced 3D Time-of-Flight MR Angiography As Compared with Fat-Suppressed MR Imaging Techniques

René van den Berg, Berit M. Verbist, Bart J. A. Mertens,
Andel G. L. van der Mey, and Mark A. van Buchem

BACKGROUND AND PURPOSE: **MR imaging techniques have proved their efficacy in imaging the head and neck region. In this study, we compared T1-weighted, dual T2-weighted, and fat-suppressed MR imaging and unenhanced and contrast-enhanced 3D time-of-flight MR angiography sequences for detection of head and neck paragangliomas.**

METHODS: **Thirty-one patients with 70 paragangliomas were examined. Four combinations of MR images were reviewed by two neuroradiologists: T1-weighted and dual T2-weighted fast spin-echo images, T1- and T2-weighted fat-suppressed fast spin-echo images, T1-weighted and contrast-enhanced T1-weighted fat-suppressed spin-echo images, and unenhanced and contrast-enhanced 3D time-of-flight MR angiograms. The randomized examinations were independently evaluated for image quality, presence of tumor, tumor size, and intratumoral flow signal intensity. The standard of reference for presence of tumor was digital subtraction angiography. Data were analyzed by using the logistic regression method.**

RESULTS: **Mean sensitivity, specificity, and negative predictive values, respectively, were assessed by the two observers to be as follows: for dual T2-weighted fast spin-echo, 74%/99%/86%; for T2-weighted fat-suppressed fast spin-echo, 70%/100%/85%; for contrast-enhanced T1-weighted fat-suppressed spin-echo, 73%/100%/86%; and for unenhanced and contrast-enhanced 3D time-of-flight MR angiography, 89%/99%/93%. Sensitivity was significantly better for unenhanced and contrast-enhanced 3D time-of-flight MR angiography ($P = .000028$). More intratumoral flow signal intensity was depicted with unenhanced and contrast-enhanced 3D time-of-flight MR angiography.**

CONCLUSION: **A combination of unenhanced and contrast-enhanced 3D time-of-flight MR angiography is superior for detecting paragangliomas and should be added to a standard imaging protocol, especially for patients with familial paragangliomas because they are more susceptible to multicentric disease.**

Paragangliomas of the head and neck are highly vascular neoplasms originating from paraganglionic tissue located at the carotid bifurcation (carotid body tumors), along the nodose ganglia of the vagus nerve (vagal paragangliomas), and in the jugular fossa and tympanic cavity (jugulotympanic paragangliomas). In general, imaging techniques are used for patients with (suspected) paragangliomas for three reasons: 1) to analyze the condition of a patient who presents with a mass lesion in the neck, a bruit, or a cranial nerve deficit, in whom a paraganglioma is suspected; 2) to monitor the size and extension of paragangliomas in patients with known paragangliomas for whom a wait-and-image policy is proposed (1, 2); 3) to screen asymptomatic kindred of patients with hereditary paragangliomas who are at risk for developing paragangliomas.

In the past, diagnostic angiography played an important role as a first-line imaging investigation for paragangliomas. Since the advent of CT and MR imaging, however, such an invasive study is reserved for those few patients whose diagnosis, after sectional

Received July 21, 2003; accepted after revision October 6.

From the Departments of Radiology (R.v.d.B., B.M.V., M.A.v.B.) and Otolaryngology (A.G.L.v.d.M.), Leiden University Medical Center, and the Department of Medical Statistics (B.J.A.M.), University of Leiden, Leiden, the Netherlands.

Address reprint requests to René van den Berg, MD, Department of Radiology, C2-S, Leiden University Medical Center, PO Box 9600, 2300 RC Leiden, the Netherlands.

TABLE 1: Imaging parameters of the sequences used

	TR	TE	NSA	Flip Angle (degrees)	Section Thickness (mm)	FOV	RFOV	Matrix	Imaging Time
T1W-SE	600	20	2	90	5 (gap, 1)	250	70	205 × 256	5:49
T2W-FSE	3750	28/120	3	90	5 (gap, 1)	240	91	177 × 256	4:56
T2W-FS-FSE	5500	100	2	90	5 (gap, 1)	250	91	177 × 256	3:45
CE-T1W-FS-SE	625	17	2	90	5 (gap, 1)	250	70	179 × 256	5:19
3D TOF MRA	25	6.9	1	20	1.5	210	70	196 × 256	5:52

Note.—NSA indicates number of signal averages; FOV, field of view; RFOV, rectangular field of view; T1W-SE, T1-weighted spin-echo; T2W-FSE, dual T2-weighted fast spin-echo; T2W-FS-FSE, T2-weighted fat-suppressed fast spin-echo; CE-T1W-FS-SE, contrast-enhanced T1-weighted fat-suppressed spin-echo; 3D TOF MRA, unenhanced and contrast-enhanced 3D time-of-flight MR angiography.

imaging, remains inconclusive (3). High resolution CT might have an advantage over MR imaging in depicting small tympanic paragangliomas (4, 5), but for most other localizations, MR imaging is preferred because of the superior soft tissue differentiation, which not only facilitates tumor detection but also improves tumor characterization and assessment of tumor extension (4, 6). In cases of skull base paragangliomas, CT and MR imaging can be complementary imaging techniques, especially before surgical resection (7).

In 1994, van Gils et al (8) showed that conventional unenhanced and contrast-enhanced T1-weighted and dual T2-weighted MR imaging sequences lack a high enough sensitivity to detect paragangliomas. Since then, a multitude of sequences to investigate head and neck lesions have become available. Fat-suppressed MR imaging techniques have proved their efficacy for the detection of mass lesions in the head and neck region (7, 9–11), and 3D time-of-flight MR angiography is capable of visualizing paragangliomas (12, 13). In this study, we compared combinations of T1-weighted spin-echo and dual T2-weighted fast spin-echo sequences, T1-weighted spin-echo and T2-weighted fat-suppressed fast spin-echo sequences, T1-weighted spin-echo and contrast-enhanced fat-suppressed T1-weighted sequences, and an unenhanced and contrast-enhanced 3D time-of-flight MR angiography sequence in terms of ability to visualize paragangliomas of the head and neck. The goal was to determine which combination of MR imaging techniques is best for detection and characterization of the tumors. Special attention was paid to the capability of these techniques to show intratumoral flow because this is one of the characteristic features of paragangliomas that permits differentiation from other tumors such as schwannomas. Finally, detection of small (<10 mm) paragangliomas was part of the analysis because in multicentric disease, these additional lesions can influence patient care. The standard of reference was digital subtraction angiography.

Methods

Patients

Patients with paragangliomas are referred to our institution for clinical evaluation, genetic counseling, and radiologic imaging. During a 2-year period from October 1998 until October 2000, 87 consecutive patients with positive family histories of paragangliomas, suspicion of having paragangliomas, or already proved paragangliomas (imaged to determine tumor growth) were examined by using a standard MR imaging protocol, as described below. Thirty-one of the 87 patients underwent digital subtraction angiography, either to confirm the diagnosis or as part of the preoperative workup (embolization) for paraganglioma. Only these 31 patients were included in this study. The group consisted of 23 female and eight male patients with a median age of 42 years (age range, 26–61 years). Twenty-four patients with paragangliomas were regarded as having familial disease based on positive gene findings. For 17 patients, digital subtraction angiography was performed before MR imaging (time range, 1−40 months; mean interval, 19 months). For the other 14 patients, digital subtraction angiography was performed after MR imaging (time range, 1−22 months; mean interval, 6 months). None of these patients underwent surgery during the period between digital subtraction angiography and MR imaging.

MR Imaging Sequences

Imaging was performed on an MR imaging system that operated at a field strength of 1.5 T (Philips Medical Systems, Best, the Netherlands) with a standard quadrature neck coil. The imaging protocol included T1-weighted spin-echo, dual T2-weighted fast spin-echo, T2-weighted fat-suppressed fast spin-echo, contrast-enhanced T1-weighted fat-suppressed spin-echo, and unenhanced and contrast-enhanced 3D time-of-flight MR angiography sequences. The imaging parameters are presented in Table 1. A gradient-echo technique with five overlapping slabs and a cranially placed slab for saturation of venous flow was used for unenhanced and contrast-enhanced 3D time-of-flight MR angiography. All imaging sequences covered an area proximal from the carotid bifurcation to the skull base region.

Image Interpretation

Combinations of MR imaging sequences were presented in random order to two neuroradiologists (R.v.d.B., B.M.V.) for independent evaluation. Only the axial view images were used in this study. A combination of T1-weighted spin-echo and dual T2-weighted fast spin-echo imaging techniques was considered to be a clinical routine used as standard sequences. T2-weighted fat-suppressed fast spin-echo imaging was combined with T1-weighted spin-echo imaging because anatomic landmarks are more difficult to appreciate on the T2-weighted fat-suppressed fast spin-echo images. To determine tumor enhancement, contrast-enhanced T1-weighted fat-suppressed spin-echo imaging was combined with T1-weighted spin-echo imaging. To determine tumor enhancement on 3D time-of-flight MR angiograms, only the unenhanced and contrast-enhanced sequences were used, without an additional T1-weighted spin-echo sequence. The observers were unaware of clinical information and other patient data. To eliminate the potential effect of a learning curve, the first 10 data sets were presented a second time at the end of the reading sessions.

Only the second reading of these data sets was used for statistical analysis. The time available for interpreting the images was unrestricted.

First, the overall image quality was considered. It was assessed whether the anatomic coverage was appropriate, from carotid bifurcation to the skull base region, and whether the technical quality was acceptable for diagnosis. Furthermore, the readers were asked to determine the presence or absence of pulsation artifacts, susceptibility artifacts, and ghosting artifacts.

For each possible tumor location on both sides (ie, carotid body tumors, vagal paragangliomas, and jugulotympanic paragangliomas), the readers were asked to assess their degree of confidence for the presence or absence of a tumor by using a 5-point scale: 1, definitely present; 2, probably present; 3, equivocal; 4, probably absent; 5, definitely absent. A carotid body tumor was defined as a lesion splaying the carotid bifurcation, displacing the internal carotid artery posteriorly and the external carotid artery anteriorly. Vagal paragangliomas were defined as lesions in the carotid space, causing anterior displacement of the internal carotid artery. Jugulotympanic paragangliomas are located near the jugular fossa or the middle ear. Both vagal and jugulotympanic paragangliomas can extend through the jugular foramen. Extension in the jugular foramen itself was not considered as a multicentric lesion, but when a paraganglioma was a contiguous lesion, cranial and caudal to the jugular foramen, it was considered as two separate lesions.

Readers were required to specify the caudal and cranial borders of the tumor by providing the respective section numbers. For analysis of the results, this information was used to verify whether they detected the same lesions. When readers correctly identified the tumor but misclassified the tumor in terms of type (carotid, vagal, jugulotympanic), a correction was made afterward to eliminate the influence of misclassification on the results.

Tumor size was determined both in the axial plane and in the craniocaudal direction. The average value was used to divide tumors according to size in five subgroups: ≤10 mm, 11–20 mm, 21–30 mm, 31–50 mm, and ≥51 mm. Other features assessed were presence or absence of flow voids and tumor extension through the jugular foramen.

The standard of reference in this study was digital subtraction angiography. Digital subtraction angiography consisted of selective injection of the common carotid and vertebral arteries and additional injections of the external carotid artery. All angiograms were obtained in anteroposterior and lateral directions. Whether tumor was shown on digital subtraction angiograms was determined after the MR image reading sessions (R.v.d.B.).

Statistical Analysis

Because distribution among the different confidence levels was poor, the results were dichotomized for data analysis. Readings were considered positive for confidence levels of definitely and probably present; the other levels were considered negative (absence of tumor). Sensitivity, specificity, and negative predictive values were calculated for each observer separately, and from both values, a mean was calculated. These values were calculated in terms of presence or absence of tumor at each of the six possible tumor localizations and do not reflect the presence or absence of disease in a patient. Because we determined sensitivity and specificity in a population of patients who were all known to have paragangliomas, the resulting figures should be interpreted with caution. This study was designed for comparing the diagnostic potential of different sets of MR imaging sequences. The sensitivity and specificity figures cannot be extrapolated to a mixed population of patients with and those without paragangliomas.

A logistic regression model was fitted for the probability to detect a paraganglioma, which used the MR imaging sequence as a predictor variable (14, 15). From these data and by using this model, odds ratios were calculated to compare the relative efficacy of the respective sequences in detecting abnormality. The likelihood ratio test was used to compare sensitivity and specificity between different techniques. A random effects version of the logistic regression model was also recalculated to take into account and evaluate the effects of between-observer variability on the model-based evaluations. Furthermore, sensitivity by tumor localization was calculated and presence of tumor in relation to tumor size was determined.

Results

Tumor Distribution and Characteristics

Seventy paragangliomas were detected with digital subtraction angiography, comprising 36 carotid body tumors, 21 vagal paragangliomas, and 13 jugulotympanic paragangliomas. Eight patients had solitary paragangliomas. Twenty-three patients (74%) had multiple paragangliomas: 12 with two each, eight with three each, two with four each, and one with six. Multicentricity was more frequently observed in familial paragangliomas (19 of 24 patients) than in nonfamilial paragangliomas (four of seven patients).

Nine paragangliomas were ≤10 mm in diameter (maximum dimension): six carotid body tumors, one vagal paraganglioma, and two jugulotympanic paragangliomas. Nineteen paragangliomas measured between 11 and 20 mm, 12 between 21 and 30 mm, and 22 between 31 and 50 mm, and eight were ≥51 mm.

Image Quality

For all patients, appropriate anatomic coverage was obtained and the technical quality was appropriate for assessment. Pulsation artifacts were seen more often on T2-weighted fat-suppressed fast spin-echo images (52%) than on the other types of images (contrast-enhanced T1-weighted fat-suppressed spin-echo images, 26%; dual T2-weighted fast spin-echo images, 16%; unenhanced and contrast-enhanced 3D time-of-flight MR angiograms, 13%). Susceptibility artifacts were observed twice with contrast-enhanced T1-weighted fat-suppressed spin-echo images. Ghosting artifacts were especially seen on dual T2-weighted fast spin-echo images (55%) and T2-weighted fat-suppressed fast spin-echo images (29%).

Tumor Detection

Sensitivity, specificity, and negative predictive values were calculated. Values are presented for each reader separately and for both readers together (Table 2). Both readers detected more paragangliomas by using unenhanced and contrast-enhanced 3D time-of-flight MR angiography than by using the other techniques. When fitting a logistic regression model to compare sensitivity to detect abnormality, odds ratios approximately equal to 1 were found for dual T2-weighted fast spin-echo, T2-weighted fat-suppressed fast spin-echo, and contrast-enhanced T1-weighted fat-suppressed spin-echo imaging, suggesting that no significant differences exist among these

TABLE 2: Data regarding sensitivity, specificity, and negative predictive value [mean (observer 1 − observer 2)]

	Sensitivity	Fitted Probability*	Odds*	Specificity	NPV
T2W-FSE	0.74 (0.64 − 0.83)	.735	2.783	0.99 (1.00 − 0.97)	0.86
T2W-FS-FSE	0.70 (0.64 − 0.76)	.699	2.333	1.00 (1.00 − 1.00)	0.85
CE-T1 W-FS-SE	0.73 (0.67 − 0.79)	.738	2.683	1.00 (1.00 − 1.00)	0.86
3D TOF MRA	0.89 (0.87 − 0.90)	.917	7.749	0.99 (0.99 − 0.99)	0.93

* Fitted probability and odds determined with logistic regression model.

Note.—NPV indicates negative predictive value; T2W-FSE, dual T2-weighted fast spin-echo; T2W-FS-FSE, T2-weighted fat-suppressed fast spin-echo; CE-T1W-FS-SE, contrast-enhanced T1-weighted fat-suppressed spin-echo; 3D TOF MRA, unenhanced and contrast-enhanced 3D time-of-flight MR angiography.

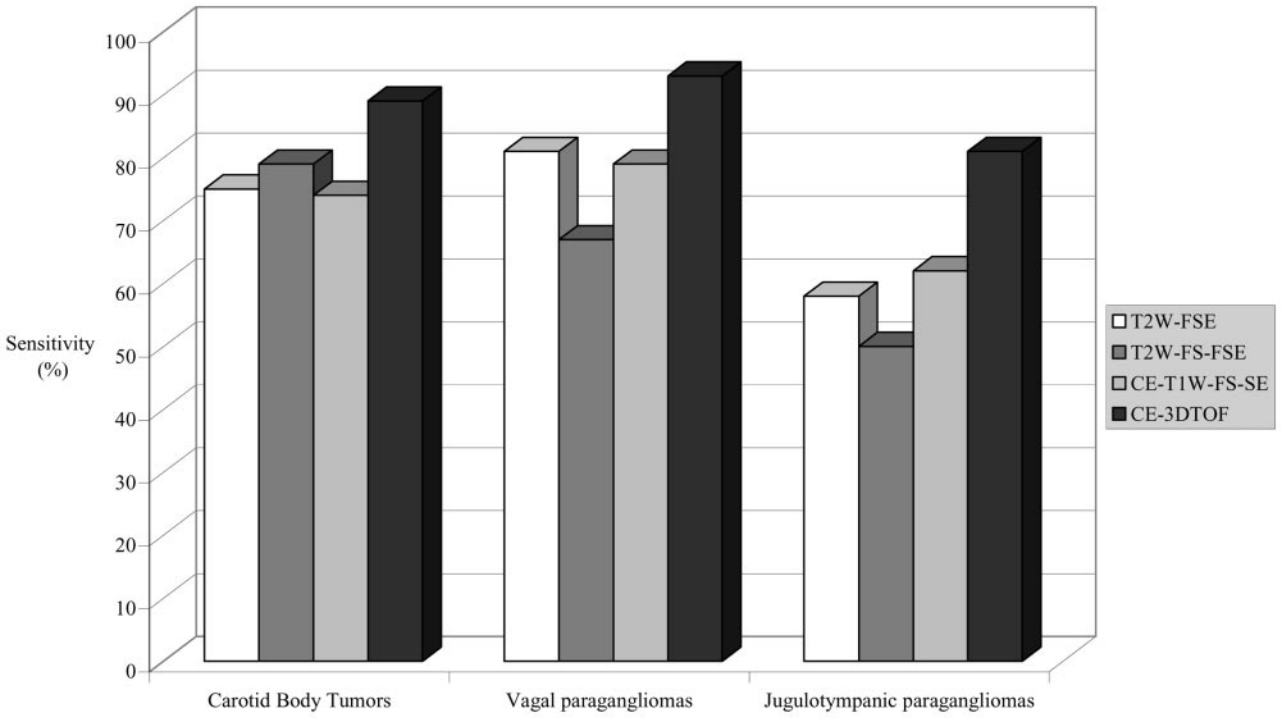

FIG 1. Bar graph shows sensitivity (mean for both observers) for detection of carotid body tumors, vagal paragangliomas, and jugulotympanic paragangliomas for each MR imaging technique. *T2W-FSE*, T2-weighted fast spin-echo imaging; *T2W-FS-FSE*, T2-weighted fat-suppressed fast spin-echo imaging; *CE-T1W-FS-SE*, contrast-enhanced T1-weighted fat-suppressed spin-echo imaging; *CE-3DTOF*, contrast-enhanced 3D time-of-flight imaging.

three techniques. We did, however, subsequently find odds ratios of approximately 3 for any comparison of unenhanced and contrast-enhanced 3D time-of-flight MR angiography versus any of the other three techniques, which suggests considerable improvement in detecting paragangliomas. The likelihood ratio test for this comparison (with 1 degree of freedom) was statistically significant ($P = .000028$). The results were found to be not much affected by between-observer variance, as could be determined from a recalculation of the same model to take the interobserver differences into account. In other words, observer variability did not seem to influence test results. The unenhanced and contrast-enhanced 3D time-of-flight MR angiography sequence also showed the highest negative predictive value.

Next, mean sensitivity for both observers was calculated per tumor localization (Fig 1). Carotid body tumors and vagal paragangliomas were better detected than jugulotympanic paragangliomas. Regarding the 13 jugulotympanic paragangliomas, one observer missed two tumors that were ≤10 mm with unenhanced and contrast-enhanced 3D time-of-flight MR angiography and the other observer missed three such small tumors. Each of these patients had two or more concomitant tumors. For all localizations, unenhanced and contrast-enhanced 3D time-of-flight MR angiography performed better than did the other techniques.

When tumor detection was related to size, detection was especially poor for lesions ≤10 mm (Table 3) at all three tumor localizations. With unenhanced and contrast-enhanced 3D time-of-flight MR angiography, each observer detected only two and four of nine paragangliomas, respectively, in this subgroup of smaller tumors (Fig 2). When we translate these numbers to the total group of paragangliomas, this means that a total of 12 tumors ≤10 mm were missed by the two observers. This will decrease mean sensitivity for the total group of tumors to 9% (12 of 140 tumors).

TABLE 3: Number of detected tumors (mean for observers 1 and 2) in relation to tumor size for each MR imaging technique as compared with criterion standard DSA

	0–10 mm	11–20 mm	21–30 mm	31–50 mm	≥51 mm
T2W-FSE	1 (0)	11 (3)	10 (2)	22 (17)	8 (8)
T2W-FS-FSE	1 (0)	9 (2)	11 (3)	21 (17)	8 (7)
CE-T1 W-FS-SE	1 (0)	11 (2)	10 (0)	22 (16)	8 (8)
CE-3D TOF	3 (1)	17 (11)	12 (10)	22 (20)	8 (8)
DSA	9	19	12	22	8

Note.—T2W-FSE indicates dual T2-weighted fast spin-echo; T2W-FS-FSE, T2-weighted fat-suppressed fast spin-echo; CE-T1 W-FS-SE, contrast-enhanced T1-weighted fat-suppressed spin-echo; 3D TOF MRA, unenhanced and contrast-enhanced 3D time-of-flight MR angiography; DSA, digital subtraction angiography. Data in parenthesis represent presence of intra-tumoral flow for each subgroup and technique.

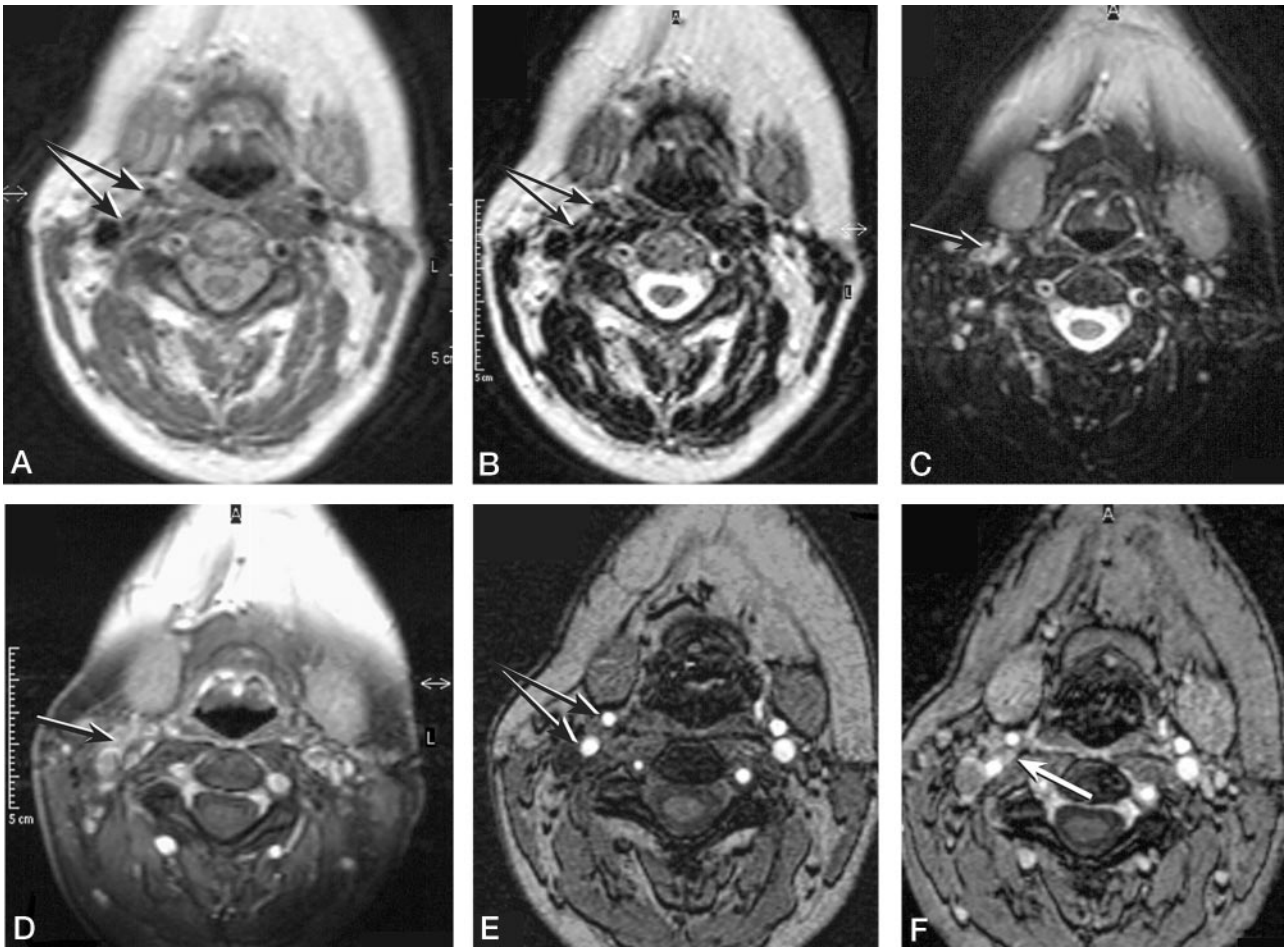

FIG 2. Images of a 51-year-old woman with a small right-sided carotid body tumor (confirmed angiographically) and a large left-sided vagal paraganglioma (not shown).

A and *B*, Axial view dual T2-weighted fast spin-echo image (3750/28/120 [$TR/TE_1/TE_2$]) shows only slight splaying of the carotid bifurcation (*double arrow*).

C, On the axial view T2-weighted fat-suppressed fast spin-echo image (5500/100 [TR/TE]), neither the carotid bifurcation nor a carotid body tumor is visible. High signal intensity in the carotid region is reflecting slow venous flow (*arrow*).

D, On the axial view contrast-enhanced T1-weighted fat-suppressed spin-echo image (625/17 [TR/TE]), enhancement of veins surrounding the normal left-sided carotid bifurcation (*arrow*) constrains detection of the small carotid body tumor (*arrow*).

E, Splaying of the carotid bifurcation (*double arrow*) can be noticed on the axial view unenhanced 3D time-of-flight MR angiogram (25/6.9/20 [TR/TE/flip angle]).

F, Enhancement of a small carotid body tumor (*arrow*) is depicted on the axial view contrast-enhanced 3D time-of-flight MR angiogram (25/6.9/20).

One 30-mm paraganglioma was not detected by either observer. The missed vagal paraganglioma was contiguous with a large carotid body tumor, but both observers failed to detect this as a separate tumor with the T2-weighted fat-suppressed fast spin-echo technique.

The presence of flow voids was determined and related to tumor size (Table 3). Unenhanced and contrast-

enhanced 3D time-of-flight MR angiography showed more intratumoral flow signal intensity than did the other MR imaging techniques for tumors that were 11 to 30 mm. Only one of nine tumors ≤10 mm showed flow signal intensity. Two of the 22 lesions measuring 31 to 50 mm did not show intratumoral flow signal intensity.

Discussion

The results of this study show that a combination of unenhanced and contrast-enhanced 3D time-of-flight MR angiography is superior to the other tested combinations of techniques in the detection of head and neck paragangliomas, independent of localization and size of the paraganglioma. This can be attributed to several factors.

The first and main advantage of unenhanced and contrast-enhanced 3D time-of-flight MR angiography over other imaging techniques is that the region of interest can be imaged with thin, overlapping sections. The other techniques display small lesions (<10 mm) only on one or two sections. With unenhanced and contrast-enhanced 3D time-of-flight MR angiography, such small lesions can be seen on more sections, increasing the diagnostic accuracy. Analysis of our results shows that paragangliomas ≤10 mm were very difficult to detect, even with unenhanced and contrast-enhanced 3D time-of-flight MR angiography. This can be attributed to the size itself, but it is important to note that these small tumors were always concomitant lesions. The better performance of unenhanced and contrast-enhanced 3D time-of-flight MR angiography as compared with the other MR imaging techniques is especially true for lesions measuring 10 to 20 mm. The higher overall sensitivity for 3D time-of-flight MR angiography is the result of the better detection of tumors measuring 10 to 20 mm. The lower sensitivity of jugulotympanic paragangliomas should not be attributed to the localization of the tumor but to the relatively high number of tumors ≤10 mm (three of 13 tumors).

Second, both unenhanced and contrast-enhanced MR angiograms show the inflow of blood in the lesion, hence increasing the signal intensity of the highly vascular tumor bed, whereas the short TR of the technique saturates the signal intensity of the surrounding soft tissue structures in the neck. Paragangliomas ≤20 mm lack sufficient intratumoral flow; it therefore might be more difficult to detect these lesions by using only unenhanced 3D time-of-flight MR angiography. Administration of gadopentetate dimeglumine will cause significant enhancement of these highly vascular lesions; as a result, tumor detection will improve when these unenhanced and contrast-enhanced 3D time-of-flight MR angiograms can be compared (Fig 2E and F).

Third, enlarged feeding arteries are a secondary sign drawing attention to a vascular lesion such as a paraganglioma. These arteries can be followed on the consecutive images toward the tumor, allowing better detection of difficult-to-delineate tumors (12). Fourth, unenhanced and contrast-enhanced 3D time-of-flight MR angiograms suffer the least from pulsation artifacts.

The lack of improvement in detecting paragangliomas with fat-suppressed techniques compared with T1-weighted spin-echo and dual T2-weighted fast spin-echo sequences in this study was especially remarkable regarding jugulotympanic paragangliomas. The high signal intensity of the bone marrow in the petrous bone easily obscures paragangliomas in this region, and fat suppression should increase the detection rate significantly. However, the results from this study showed no increase in detection when fat-suppressed techniques were compared with dual T2-weighted fast spin-echo imaging (Fig 3), which is not in concordance with what has been described for pharyngeal and skull base abnormalities. Previous reports stated that both contrast-enhanced T1-weighted fat-suppressed spin-echo imaging (16) and T2-weighted fat-suppressed fast spin-echo imaging (10, 11) show better tumor delineation compared with conventional

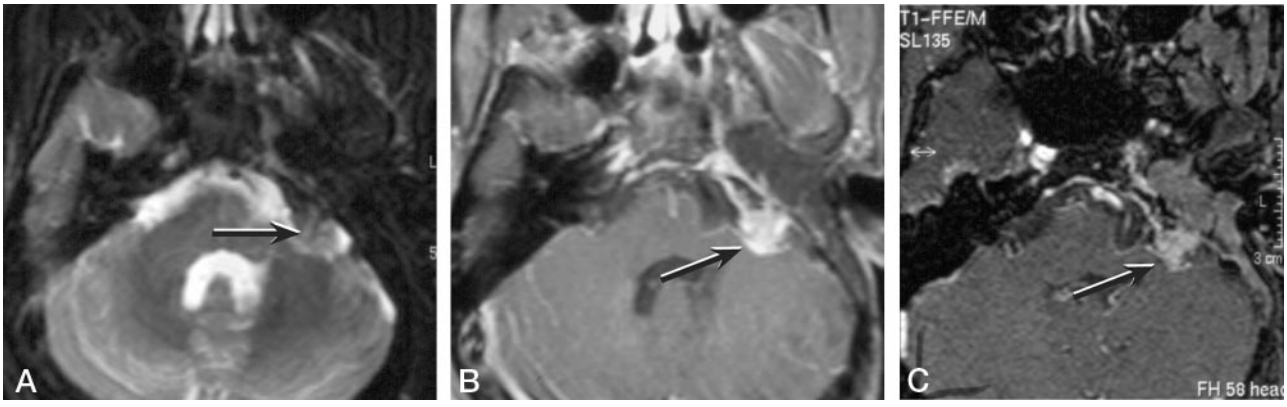

FIG 3. Images of a 35-year-old man after surgical resection of a left-sided jugulotympanic paraganglioma with a small residual lesion in the left cerebellopontine angle.

A, Residual paraganglioma in the left cerebellopontine angle is not clearly depicted with the T2-weighted fat-suppressed fast spin-echo sequence (5500/100 [TR/TE]).

B, Contrast-enhanced T1-weighted fat-suppressed spin-echo image (625/17 [TR/TE) clearly shows a small residual paraganglioma (*arrow*).

C, Contrast-enhanced 3D time-of-flight MR angiogram (25/6.9/20 [TR/TE/flip angle]) clearly shows a small residual paraganglioma (*arrow*).

fast spin-echo imaging, with a better performance of T2-weighted fat-suppressed fast spin-echo imaging than with contrast-enhanced T1-weighted fat-suppressed spin-echo imaging (17). However, when considering detection of tumors in the pharynx, no improvement was observed when comparing contrast-enhanced T1-weighted fat-suppressed spin-echo with unenhanced T1-weighted spin-echo images (9). Paragangliomas exhibit a different (intermediate) signal intensity on T1- and T2-weighted images (3) compared with the high signal intensity of squamous cell carcinomas on T2-weighted images. This difference in signal intensities might explain the different outcome of this study.

Susceptibility artifacts did not play a role in reducing the diagnostic performance of the contrast-enhanced T1-weighted fat-suppressed spin-echo sequence in the skull base region. However, in the cervical region, fat suppression images were degraded by pulsation artifacts. These artifacts are especially present on the images of this patient group because of the highly vascular nature of the tumor with resulting enlargement of the branch arteries of the external carotid artery supplying these lesions. In a case of bilateral tumors, the smaller tumor can be obscured because of these artifacts.

Dynamic contrast-enhanced MR imaging has previously been described as a technique to identify paragangliomas (18). Furthermore, it has proved efficacious in delineating the margins and extent of several other head and neck tumors (19). This technique is especially useful for differentiating paragangliomas from other head and neck tumors. Paragangliomas show a typical dropout effect after the administration of gadopentetate dimeglumine (0.3 mmol/kg), caused by the strong enhancement of this highly vascular tumor. A high temporal resolution of 2 s per image is necessary to show this enhancement pattern. The limitation of this technique, however, is the number of sections that can be acquired. When screening for head and neck paragangliomas, the region of interest should at least cover an area of 10 cm from the carotid bifurcation to the skull base. When the number of sections imaged has to increase, this will reduce the temporal resolution. This will result in more pronounced enhancement of venous structures, and such enhancement might obscure (additional) small lesions.

Because our institution is a referral center for patients with (familial) paragangliomas, the number of patients studied with the use of MR imaging is disproportionately high compared with other institutions. For this population, we sought an imaging technique approaching the diagnostic performance of digital subtraction angiography. The specific referral pattern might introduce a bias in the population of this study. However, because all patients underwent the same MR imaging protocol and because reading of the images was standardized, this bias probably did not affect the outcome.

The prevalence of multicentricity in both the nonfamilial (57%) and familial (79%) groups of patients in this study was higher than the prevalence of 10% and 25% to 50%, respectively, previously described (20). This high prevalence can be attributed to patient selection. A conservative wait-and-image policy is more amenable for patients with multiple lesions. These patients underwent frequent MR imaging and had a higher chance to undergo MR imaging during the period when patients were enrolled in the study than did patients with single tumors, as these solitary tumors are often surgically resected after the diagnosis has been made (21, 22). The combinations of paragangliomas found most frequently were bilateral carotid body tumors. Furthermore, carotid body tumors and vagal paragangliomas were often present together. The combination of a jugulotympanic paraganglioma with any other localization was much less frequently observed in this study group, in contrast with what has been reported previously (23). The detection of multicentric disease is important because it is the most important determinant in the treatment of these patients (22, 24).

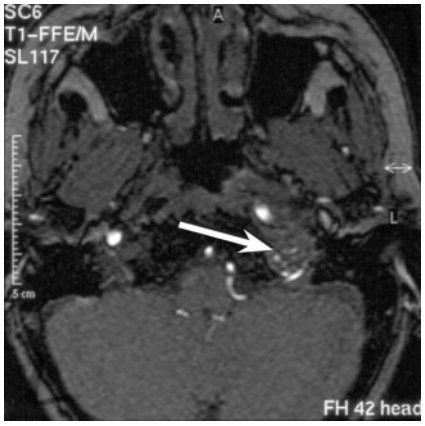

FIG 4. Unenhanced 3D time-of-flight MR angiogram (25/6.9/20 [TR/TE/flip angle]) of a 39-year-old woman with a left-sided jugulotympanic paraganglioma clearly shows the highly vascular nature of the lesion (*arrow*).

Certain MR imaging characteristics can help differentiate paragangliomas from other tumors in the head and neck region. The specific localization of each type of paraganglioma in relation to the internal carotid artery (25), the jugular bulb, or the petrous bone (middle ear) already should raise the suspicion but is not pathognomonic, as nerve sheath tumors can be localized in the same regions. The flow signal intensity within the tumor, however, makes differentiation from schwannomas possible (Fig 4). Other vascular tumors in the head and neck region, such as hemangiopericytomas and metastases from highly vascular tumors (eg, renal cell carcinoma), can mimic paragangliomas because of their intratumoral flow signal intensity, but the more a-specific localization (ie, more random distribution not linked to predetermined localization) of such lesions makes the diagnosis of paraganglioma much less probable. In addition, the detection of multiple lesions in the typical localizations further increases the likelihood that the lesion is a paraganglioma. In this study, unenhanced

and contrast-enhanced 3D time-of-flight MR angiography was superior to the other techniques to depict multicentric disease and flow voids; with this technique, the diagnosis paraganglioma could be established with a very high degree of certainty.

In conclusion, the following diagnostic strategy can be recommended for patients with symptomatic head and neck lesions. If unenhanced T1- and T2-weighted images raise the suspicion of a paraganglioma, unenhanced and contrast-enhanced 3D time-of-flight MR angiography should be added because it can provide essential information regarding the vascular nature of the tumor and is better able to show multicentric disease. Unenhanced and contrast-enhanced 3D time-of-flight MR angiography alone can be used for screening and follow-up of patients with a positive family history of paragangliomas.

References

1. Jansen JC, van den Berg R, Kuiper A, van der Mey AG, Zwinderman AH, Cornelisse CJ. **Estimation of growth rate in patients with head and neck paragangliomas influences the treatment proposal.** *Cancer* 2000;88:2811–2816
2. van der Mey AG, Frijns JH, Cornelisse CJ, et al. **Does intervention improve the natural course of glomus tumors? a series of 108 patients seen in a 32-year period.** *Ann Otol Rhinol Laryngol* 1992; 101:635–642
3. Som PM, Curtin HD. **Lesions of the parapharyngeal space: role of MR imaging.** *Otolaryngol Clin North Am* 1995;28:515–542
4. Rao AB, Koeller KK, Adair CF. **From the archives of the AFIP: paragangliomas of the head and neck: radiologic-pathologic correlation: Armed Forces Institute of Pathology.** *Radiographics* 1999; 19:1605–1632
5. Phelps PD, Cheesman AD. **Imaging jugulotympanic glomus tumors.** *Arch Otolaryngol Head Neck Surg* 1990;116:940–945
6. Olsen WL, Dillon WP, Kelly WM, Norman D, Brant-Zawadzki M, Newton TH. **MR imaging of paragangliomas.** *AJR Am J Roentgenol* 1987;148:201–204
7. Noujaim SE, Pattekar MA, Cacciarelli A, Sanders WP, Wang AM. **Paraganglioma of the temporal bone: role of magnetic resonance imaging versus computed tomography.** *Top Magn Reson Imaging* 2000;11:108–122
8. van Gils AP, van den Berg R, Falke TH, et al. **MR diagnosis of paraganglioma of the head and neck: value of contrast enhancement.** *AJR Am J Roentgenol* 1994;162:147–153
9. Barakos JA, Dillon WP, Chew WM. **Orbit, skull base, and pharynx: contrast-enhanced fat suppression MR imaging.** *Radiology* 1991;179:191–198
10. Lewin JS, Curtin HD, Ross JS, Weissman JL, Obuchowski NA, Tkach JA. **Fast spin-echo imaging of the neck: comparison with conventional spin-echo, utility of fat suppression, and evaluation of tissue contrast characteristics.** *AJNR Am J Neuroradiol* 1994;15: 1351–1357
11. Panush D, Fulbright R, Sze G, Smith RC, Constable RT. **Inversion-recovery fast spin-echo MR imaging: efficacy in the evaluation of head and neck lesions.** *Radiology* 1993;187:421–426
12. van den Berg R, van Gils AP, Wasser MN. **Imaging of head and neck paragangliomas with three-dimensional time-of-flight MR angiography.** *AJR Am J Roentgenol* 1999;172:1667–1673
13. Vogl TJ, Juergens M, Balzer JO, et al. **Glomus tumors of the skull base: combined use of MR angiography and spin-echo imaging.** *Radiology* 1994;192:103–110
14. Cox DR, Snell EJ. *Analysis of Binary Data.* 2nd ed. London, Chapman and Hall; 1989
15. Le Cessie S, Van Houwelingen JC. **Logistic regression for correlated binary data.** *Appl Stat* 1994;43:95–108
16. Ross MR, Schomer DF, Chappell P, Enzmann DR. **MR imaging of head and neck tumors: comparison of T1-weighted contrast-enhanced fat-suppressed images with conventional T2-weighted and fast spin-echo T2 weighted images.** *AJR Am J Roentgenol* 1994;163: 173–178
17. Dubin MD, Teresi LM, Bradley WG, et al. **Conspicuity of tumors of the head and neck on fat-suppressed MR images: T2-weighted fast-spin-echo versus contrast-enhanced T1-weighted conventional spin-echo sequences.** *AJR Am J Roentgenol* 1995;164:1213–1221
18. Vogl TJ, Mack MG, Juergens M, et al. **Skull base tumors: gadodiamide injection: enhanced MR imaging: drop-out effect in the early enhancement pattern of paragangliomas versus different tumors.** *Radiology* 1993;188:339–346
19. Escott EJ, Rao VM, Guitierrez JE. **Comparison of dynamic contrast-enhanced gradient-echo and spin-echo sequences in MR of head and neck neoplasms.** *AJNR Am J Neuroradiol* 1997;18:1411–1419
20. Gulya AJ. **The glomus tumor and its biology.** *Laryngoscope* 1993; 103:7–15
21. Jackson CG, Harris PF, Glasscock ME III, et al. **Diagnosis and management of paragangliomas of the skull base.** *Am J Surg* 1990; 159:389–393
22. Jackson CG. **Neurotologic skull base surgery for glomus tumors: diagnosis for treatment planning and treatment options.** *Laryngoscope* 1993;103:17–22
23. van Baars F, van den Broek P, Cremers C, Veldman J. **Familial non-chromaffinic paragangliomas (glomus tumors): clinical aspects.** *Laryngoscope* 1981;91:988–996
24. Sillars HA, Fagan PA. **The management of multiple paraganglioma of the head and neck.** *J Laryngol Otol* 1993;107:538–542
25. Alkadhi H, Schuknecht B, Stoeckli SJ, Valavanis A. **Evaluation of topography and vascularization of cervical paragangliomas by magnetic resonance imaging and color duplex sonography.** *Neuroradiology* 2002;44:83–90